Journal of Power Sources 236 (2013) 224–229

Contents lists available at SciVerse ScienceDirect

Journal of Power Sources

journal homepage: www.elsevier.com/locate/jpowsour

Carbon-rich SiCN ceramics as high capacity/high stability anode material for lithium-ion batteries

Lukas Mirko Reinold*, Magdalena Graczyk-Zajac, Yan Gao, Gabriela Mera, Ralf Riedel

Technische Universität Darmstadt, Fachbereich Material- und Geowissenschaften, Fachgebiet Disperse Feststoffe, Petersenstraße 32, 64287 Darmstadt, Germany

HIGHLIGHTS

- SiCN ceramics were investigated in terms of Li-ion storage capacity.
- Influence of microstructure on electrochemical properties of SiCN was studied.
- Oxygen to nitrogen ratio was found to be irrelevant for capacity of SiCN.
- SiCN is potential candidate to replace graphite anodes in lithium-ion batteries.
- No linear relationship between free carbon content and capacity was found for SiCN.

ARTICLE INFO

Article history:
Received 1 November 2012
Received in revised form
14 February 2013
Accepted 18 February 2013
Available online 26 February 2013

Keywords:
Lithium-ion battery
Polymer-derived ceramic
Silicon carbonitride
Anode
Polysilazane
Polysilylcarbodiimide

ABSTRACT

Two classes of preceramic polymers, namely polysilazane and polysilylcarbodiimide, with branched and linear molecular structure were pyrolyzed at 1100 °C under argon atmosphere. The resulting nanostructured polymer-derived SiCN ceramics were characterized by means of elemental analysis, X-ray diffraction, scanning electron microscopy and Raman spectroscopy. All investigated ceramics are amorphous and contain a disordered free carbon phase of 2–2.5 nm in size. Electrochemical characterization reveals that the polysilazane-derived electrodes demonstrate higher capacity and stability during subsequent lithium insertion/extraction with different currents than those of the polysilylcarbodiimide-based electrodes. The highest lithium extraction capacity of 724 mA h g^{-1} is recovered for the sample derived from branched polysilazane whereas the best polysilylcarbodiimide-derived sample recovers 612 mA h g^{-1}. Moreover, the polysilazane-derived samples deliver a higher fraction of capacity recovered below 1.5 V. The electrochemical performance is found to be dependent on the molecular structure (silazane vs. silylcarbodiimide) of the preceramic polymer, while there is no effect associated with the amount of branching (silsesquiazane vs. silazane and silsesquicarbodiimide vs. silylcarbodiimide). The influence of "micropore activity" and oxygen content on the electrochemical performance of polymer-derived silicon carbonitrides is addressed.

1. Introduction

Polymer-derived ceramics (PDCs) have recently attracted an increasing attention in view of a possible application as anode materials in lithium-ion batteries. This class of materials can exhibit capacities exceeding that of graphite and furthermore show stable cycling behavior even at elevated charge/discharge rates.

There is a clash of opinions with respect to the storage sites of lithium in PDCs. Ahn et al. claim that the mixed bond configuration (tetrahedrally coordinated silicon from SiC_4 via SiC_3O, SiC_2O_2 and $SiCO_3$ to SiO_4) of SiOC ceramics acts as major lithiation site [1], while Fukui et al. found the free carbon phase within these materials to provide the major hosting site for Li ions [2]. So far, comparing pure PDCs, most of the publications related to the electrochemical performance of PDCs have been focused on SiOC ceramics [1–5]. Even though Dahn et al. had already patented the use of silazane-derived SiCN ceramics in 1997 showing reversible discharge capacities up to 560 mA h g^{-1} [6], little research has been done on the application of these materials in lithium-ion batteries since that time. Pure PDC-based SiCN materials derived from polysilylethylenediamine have been investigated by Su et al. [7] and Feng [8]. The work of Su et al. showed a first discharge cycle capacity of 456 mA h g^{-1} but the material suffered from strong fading with cycling. This problem of capacity fading was solved by Feng who achieved capacities higher than 300 mA h g^{-1} after 30 cycles for a current rate of 160 mA g^{-1} after an additional heat treatment

* Corresponding author. Tel.: +49 (0)6151 16 6343; fax: +49 (0)6151 16 6346.
E-mail address: reinold@materials.tu-darmstadt.de (L.M. Reinold).

0378-7753/$ – see front matter © 2013 Elsevier B.V. All rights reserved.
http://dx.doi.org/10.1016/j.jpowsour.2013.02.046

of the polymer-derived SiCN material. Promising electrochemical results with regard to the capacity and stability of SiCN derived from high-carbon containing polysilylcarbodiimides have been reported by Kaspar et al. [9] and Graczyk-Zajac et al. [10]. Recently, it has been found that composite anode materials comprised of SiCN/graphite [11] and SiCN/silicon [12] demonstrate better electrochemical properties than that of pure graphite and silicon, respectively. In parallel, Ahn et al. [1] stated that the presence of nitrogen in SiOC ceramics strongly diminishes the reversible capacity. In the above report it is claimed that high capacities of 600 mA h g^{-1} can only be found for materials with a nitrogen to oxygen (N/O) ratio below 1. The results are discussed in relationship with the degree of bond covalency, Si–N being more covalent than Si–O bonds. It is suggested that lithium is sequestered in the mixed-bond structure of silicon coordinated to both oxygen and carbon. Accordingly, the replacement of oxygen by nitrogen within the amorphous network leads to a loss in the ability of these mixed bonds to reversibly bind lithium.

In this work we demonstrate that SiC(O)N materials with a N/O ratio of about 6–9.5 show outstanding electrochemical properties in view of their possible application as anodes in lithium-ion batteries. This study is focused on electrochemical investigations of four SiCN ceramics containing a high content of free carbon but derived from pre-ceramic polymers with a different molecular structure and degree of branching. For this purpose, a branched (sample GM35) and a linear (sample HN1) polysilylcarbodiimide as well as a branched (GM65) and linear (HN3) polysilazane were synthesized. As demonstrated by solid-state NMR studies, the pyrolysis of polysilazanes at 1100 °C leads to a mixed bond configuration (tetrahedrally coordinated silicon from SiC_4 via SiC_3N, SiC_2N_2 and $SiCN_3$ to SiN_4) within the amorphous SiCN ceramic [13,14]. In contrast, the pyrolysis of polysilylcarbodiimides results in the formation of amorphous nanocomposites comprised of Si_3N_4, SiC and a free carbon phase [14–19]. In particular, the emphasis of our work is focused on the relation of the molecular structure of the precursor and of the microstructure derived therefrom on the electrochemical properties of the ceramics.

2. Experimental part

The molecular structures of the synthesized preceramic polymers are presented in Fig. 1. The polyphenylvinylsilylcarbodiimide (HN1) and polyphenylvinylsilazane (HN3) consist of linear chains whereas the polyphenylsilsesquicarbodiimide (GM35) and the polyphenylsilsesquiazane (GM65) show a branched molecular structure. As previously reported, the polysilylcarbodiimides GM35 and HN1 were produced by the polycondensation reaction of chlorosilanes with bis(trimethylsilylcarbodiimide) [16,20]. The polysilazanes GM65 and HN3 were synthesized by an improved salt-free polycondensation method involving the reaction of chlorosilanes with hexamethyldisilazane.

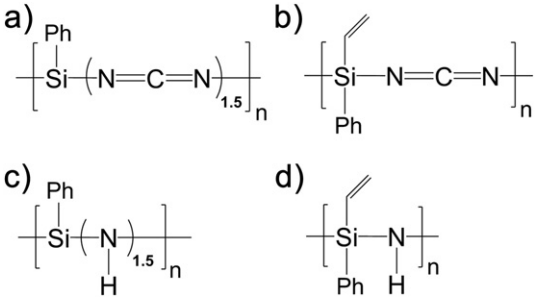

Fig. 1. Molecular structures of preceramic polymers: a) GM35, b) HN1, c) GM65 and d) HN3.

The polymers were pyrolyzed under argon at 1100 °C in a Schlenk tube in a quartz crucible. The heating and cooling rate was set to 100 °C h^{-1} and the dwelling time at 1100 °C was set to 2 h. For HN1 and HN3 an additional crosslinking step was applied at 255 °C for 5 h and 260 °C for 7 h, respectively, prior to pyrolysis. The resulting ceramics were ground and sieved with a mesh size of 40 μm. For electrode preparation a mixture of 85 wt.% of the ceramic, 5 wt.% of Carbon Black Super P® (Timcal Ltd., Switzerland) and 10 wt.% of polyvinylidenefluoride (PVdF, SOLEF, Germany) dissolved in N-methyl-2-pyrrolidone (NMP, BASF, Germany) was prepared. Additional NMP was added to adjust the viscosity of the mixture. The slurry was printed on the rough side of a copper foil (10 μm, Copper SE-Cu58 (C103), Schlenk Metallfolien, Germany) by hand and dried at 80 °C for 24 h. Electrodes of 7 mm diameter were cut out of the coated copper foil and dried at 80 °C under vacuum in a Buchi oven for 24 h. The dried electrodes were transferred without further contact to air to a glove box (MBraun, Germany) for cell assembly. For electrochemical testing a Swagelok® type cell set up was chosen. The counter/reference electrode was cut out of a metallic lithium foil (99.9% purity, 0.75 mm thickness, Alfa Aesar, Germany) with a diameter of 10 mm. QMA (Whatmann™, UK) was used as a separator and 180 μl of LP30 (Merck, Germany) was added as electrolyte.

The electrochemical testing has been performed with a VMP multipotentiostat (BioLogic Science Instruments). The same rate was used for the charge (*C*) and for the discharge (*D*) processes, $C = D$ (C/20 = 18 mA g^{-1}, C/10 = 36 mA g^{-1}, C/5 = 72 mA g^{-1}, C/2 = 180 mA g^{-1}, C/1 = 360 mA g^{-1}). By charge we consider lithium insertion, by discharge lithium extraction. All capacity calculations have been done taking into account only the active material of the electrode (being 85 wt.%). Please note, that some electrochemical results of HN1 sample have already been published in Ref. [10], though the composition of the electrodes differs strongly from the composition used in this work (no Carbon Black Super P® has been used in the previous study).

The total carbon content of the samples was determined by a combustion analysis with a carbon analyzer Leco C-200, the oxygen and nitrogen content by hot gas extraction with a N/O analyzer, Leco TC-436 (Leco Corporation, Michigan, USA). Residual hydrogen and chlorine contents of the ceramics synthesized at 1100 °C were determined at Mikroanalytisches Labor Pascher (Remagen, Germany). The silicon fraction was calculated as the difference between 100% and the analyzed values of the other elements.

SEM pictures of the pristine electrodes were taken with a Philips XL30 FEG (Philips, Netherlands). For imaging a secondary electron detector was used and the acceleration voltage was set to 10 kV.

X-ray powder diffraction of the sample HN1 was obtained in flat-sample transmission geometry on an STOE STAD1 P equipped with monochromatic Mo Kα radiation. The samples HN3, GM35 and GM65 were measured by an STOE X-ray diffractometer using Ni-filtered Cu K_α, and the scanning speed of 2θ was 7 s for 0.05°. The 2θ value of the HN1 sample which was obtained from Mo K_α radiation was recalculated as the 2θ from Cu K_α radiation, using the ratio $\lambda_{Cu}/\lambda_{Mo} = 0.15405/0.07093$.

All micro-Raman spectra (10 scans, each lasting 4 s) were recorded with a Horiba HR800 micro-Raman spectrometer (Horiba Jobin Yvon, Bensheim, Germany) equipped with an Ar laser (irradiation wavelength 514.5 nm). The excitation line has its own interference filter (to filter out the plasma emission) and a Raman notch filter (for laser light rejection). The measurements were performed with a grating of 1800 gmm^{-1} and a confocal microscope (magnification 50×, NA 0.5) with a 100 μm aperture, giving a resolution of 2–4 μm. For the evaluation of the free carbon

nanoparticle size, Gaussian curve fitting of the Raman bands (OriginPro 8.1 Software) was applied.

3. Results and discussion

3.1. Elemental analysis

The results of the elemental analysis are summarized in Table 1. The amount of silicon was calculated as the difference to 100%, assuming that no other elements are present besides C, N, O, Cl, and H. The elemental composition allows a formal calculation of the amount of free carbon present in the samples. It is assumed that oxygen is bonded to silicon as SiO_2, nitrogen and silicon form Si_3N_4 and the remaining Si is bonded to C in form of SiC. The excess carbon is assumed to exist as free carbon.

Due to the high content of nitrogen this calculation cannot be performed for sample GM35. However, NMR studies of this material showed the presence of a free carbon phase having C–N bonds at the interfaces between the amorphous Si_3N_4 phase and the free carbon phase [20].

3.2. X-ray diffraction study

X-Ray diffraction measurements revealed the amorphous nature of all of the ceramics synthesized at 1100 °C in Ar (Fig. 2).

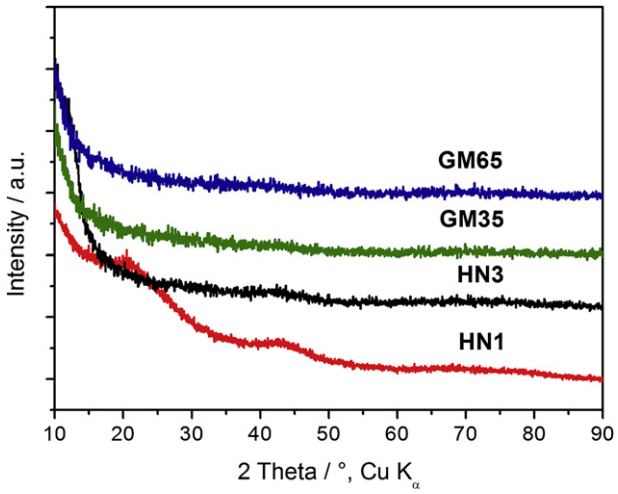

Fig. 2. X-ray diffraction patterns of the SiCN ceramics pyrolyzed at 1100 °C in Ar.

3.3. Raman spectroscopy characterization

The Raman spectra of the investigated ceramics are presented in Fig. 3. Micro-Raman spectroscopy is a nondestructive tool for the integral examination of the microstructural features of free carbon phases in PDCs. The representative bands corresponding to the free carbon phase are the so-called disorder-induced D-band at approximately 1350 cm^{-1} and the G band at approx. 1582 cm^{-1} due to in-plane bond stretching of sp^2 carbon, as well as the G′-band (the overtone of the D-band which is always observed in defect-free samples at 2700 cm^{-1}) [21–25]. The D and G bands can vary in intensity, position and width, depending on the structural organization of the sample under investigation. The intensity ratio of the D and G modes, I_D/I_G, enables the evaluation of the carbon nanoparticle size by using the formula reported by Ferrari and Robertson [21]:

$$\frac{I_D}{I_G} = C'(\lambda)L_a^2$$

L_a is the size of carbon domains along the six fold ring plane (lateral size), and C' is a coefficient that depends on the excitation wavelength of the laser. The value of the coefficient C' for the wavelength of 514.5 nm of the Ar-ion laser employed here is 0.0055 $Å^{-2}$. Gaussian curve fitting of the Raman bands was performed in order to extract the I_D/I_G intensity ratios and to determine the size of the free carbon nanoparticles formed in the ceramics. The peak fitting was done including the minor bands T (shoulder at ~1200 cm^{-1}), corresponding to the presence of sp^2 and sp^3 C–C and C=C bonds, respectively and D'' at ~1500 cm^{-1} which is assigned to the fraction of amorphous carbon [23]. The structural disorder is known to activate these forbidden vibration modes [26,27].

The lateral cluster sizes L_a in all samples are similar, between 2.01 nm (GM65) and 2.55 nm (HN3), indicating the nanostructured nature of the ceramics.

3.4. SEM pictures

Fig. 4a–d shows the SEM pictures of the pristine electrodes. The ceramic powder and the Carbon Black Super P® are homogeneously distributed and form a porous structure. No differences in the morphology among the studied samples are visible. The sieving of the ground samples lead to particle sizes below 40 μm.

3.5. Electrochemical results

For electrochemical testing various charging/discharging rates between C/20 to C/1 were applied on the cells. Fig. 5 shows the discharge capacities of the investigated materials. The best performance, with respect to the recovered capacities, was achieved with polysilazane-derived materials, HN3 and GM65. Both samples recover the outstanding capacity of 700 mA h g^{-1} for low current charge/discharge clearly exceeding the theoretical capacity of graphite. Starting with C/5 rate, the capacity of GM65 tends to fade, while it remains perfectly stable for HN3 sample. At C/1, the average discharge capacity amounts 437 mA h g^{-1} and 316 mA h g^{-1} for HN3 and GM65, respectively. The capacities recovered at low current for the polysilylcarbodiimide-derived samples are much lower, namely 612 and 486 mA h g^{-1} for HN1 and GM35, respectively. GM35 demonstrates high irreversible capacity during the first cycle, followed by stable electrochemical cycling behavior. In contrast, the ceramic derived from HN1 shows less irreversible first cycle capacity but a significant capacity fading at current rates of C/20, C/

Table 1
Results of elemental analysis. ().

Sample	O [wt.%]	N [wt.%]	C [wt.%]	Cl [wt.%]	H [wt.%]	Si [wt.%]	Empirical formula[a]	Free C [wt.%]	N/O molar ratio
HN1	2.14	14.80	56.50	1.55	0.24	24.77	$Si_1C_{5.3}O_{0.2}N_{1.2}$	56	6
HN3	2.42	13.01	52.52	0.57	0.18	31.30	$Si_1C_{3.9}O_{0.1}N_{0.8}$	48	8
GM35	3.27	25.83	35.38	6.99	0.93	27.60	$Si_1C_{3.0}O_{0.2}N_{1.9}$	–	9.5
GM65	2.13	16.04	46.86	0.03	0.35	34.59	$Si_1C_{3.2}O_{0.1}N_{0.9}$	43	9

[a] Excluding Cl and H and normalized to one silicon atom.

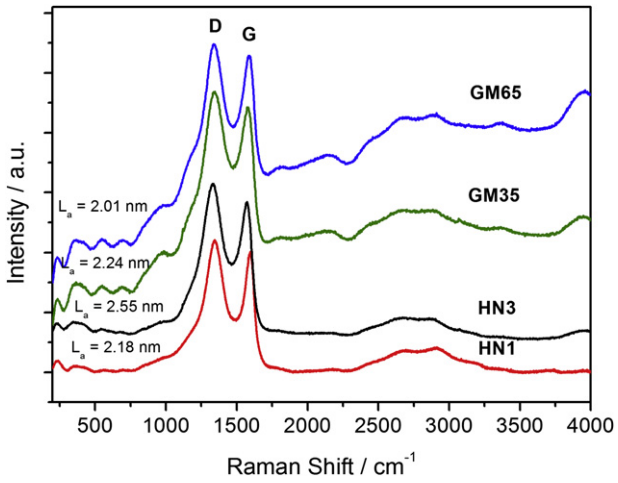

Fig. 3. Micro-Raman spectra of the SiCN ceramics pyrolyzed at 1100 °C in Ar.

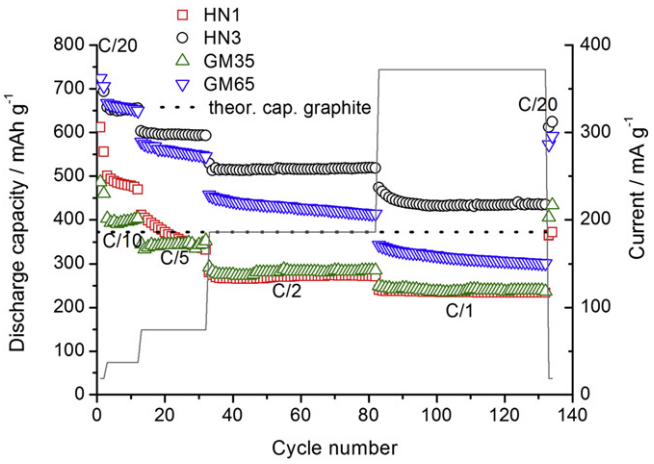

Fig. 5. Discharge capacities with corresponding rates/currents for HN1, HN3, GM35 and GM65.

10 and C/5. When finally charged/discharged with C/2 and C/1 rates, the capacity stabilizes, and the recovered capacity is similar to the one of GM35. The high irreversible capacity of GM35 during the first cycle can be attributed to the high oxygen content as well as to the presence of chlorine.

A summary of the corresponding specific capacity values for the 1st and 134th cycle is given in Table 2. The irreversible capacity $C_{irreversible}$ represents the amount of charge which is not recovered during the first discharging process and the coulombic efficiency η is given by the ratio $C_{reversible}/C_{charge}$*100%. The efficiency η' was introduced in order to evaluate the cycling stability of the material and is given by the ratio of reversible capacity recovered after 134 cycles to that after first cycle, $C_{reversible134th}/C_{reversible1st}$*100%. The averaged discharge capacities were calculated for each current step separately. All investigated ceramics exhibit promising results in terms of capacity. Our electrochemical studies clearly show no dependence of the capacity on the free carbon amount and no dependence on the N/O ratio. These results are clearly in contrast to the hypothesis that a nitrogen to oxygen ratio smaller than 1 is necessary for SiC(O)N PDCs to achieve suitable capacities [1]. According to Fig. 5 there is no difference in the discharge capacities for the sample with the highest N/O ratio (GM35) and the lowest N/O ratio (HN1). Furthermore, the cycling stability of GM35 is much better than that of sample HN1. Nevertheless, it should be pointed out that the samples investigated in Ref. [1] contain less free carbon (up to 26 wt.%) as compared to the samples reported in this work.

Figs. 6 and 7 represent the voltage–capacity dependences, both for lithium insertion and extraction, registered for the 1st and 134th cycle for polysilazanes and polysilylcarbodiimide-derived ceramics. The samples HN1, HN3 and GM65 show a plateau during the first discharge at a voltage of approximately 0.1 V. This voltage plateau has been found by Fukui et al. [2] for SiOC based anode materials and was attributed to the presence of closed micropores. GM35 reveals no “micropore activity”.

The plateaus vanish after subsequent cycling so that almost no contribution of the micropores to the capacity can be seen in the

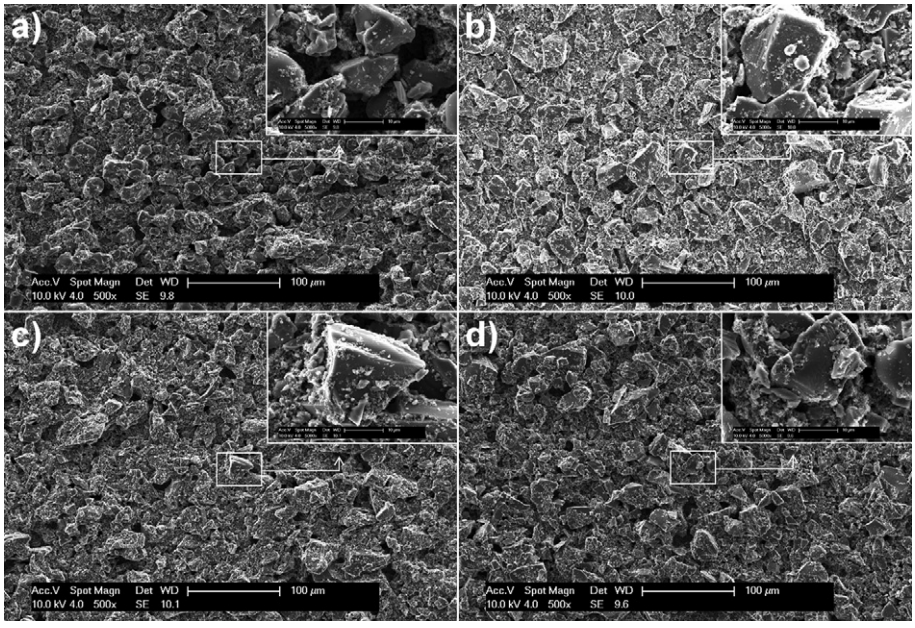

Fig. 4. SEM pictures of pristine electrodes: a) GM35, b) GM65, c) HN1 and d) HN3.

Table 2
First cycle charging/discharging capacity, irreversible capacity and coulombic efficiency, as well as averaged discharge capacities for different rates.

Sample	C_{charge} [mA h g^{-1}]	$C_{reversible}$ [mA h g^{-1}]	$C_{irreversible}$ [mA h g^{-1}]	η [%]	C/20_start [mA h g^{-1}]	C/10 [mA h g^{-1}]	C/5 [mA h g^{-1}]	C/2 [mA h g^{-1}]	C/1 [mA h g^{-1}]	C/20_end [mA h g^{-1}]	η' [%]
HN1	1033	612	421	59	584	483	365	270	235	368	61
HN3	1078	703	375	65	699	653	596	516	437	618	89
GM35	930	486	444	52	474	397	343	281	240	420	89
GM65	1211	724	487	60	715	659	559	430	316	582	82

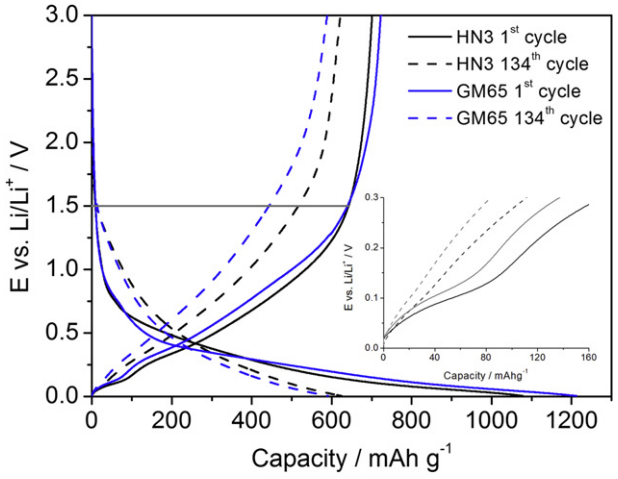

Fig. 6. 1st and 134th charge–discharge curve for the polysilazane-derived ceramics HN3 and GM65.

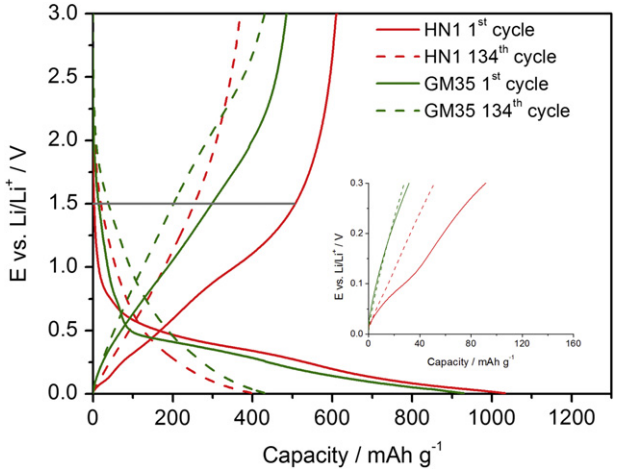

Fig. 7. 1st and 134th charge–discharge curves for the polysilylcarbodiimide-derived ceramics HN1 and GM35.

last (134th) cycle. The fading of "micropore plateau" with subsequent cycling is related to some microstructural changes in the material with ongoing insertion/extraction of lithium ions, which lead to enhanced material stability [2]. This finding corresponds to the results of the present investigation: In terms of stability expressed by η' efficiency (Table 1) the best results were obtained for the sample with the highest "micropore effect". According to this tendency, GM35 should show the lowest stability, however, η' amounts 89%. The reason for the high stability might be related to the incorporation of nitrogen in the free carbon phase but remains unclear for the moment.

Another difference in shape of the potential–capacity transients can be seen when comparing the curves of the first lithium insertion. The polysilylcarbodiimide-derived ceramics show a quasi plateau in the range of about 0.5 V whereas the polysilazane-derived materials display a curve following an exponential decay. The mentioned plateau is exclusively visible during the first cycle and does not appear anymore after further lithium insertion/extraction cycles. Interestingly, different shapes of the potential curves during the first lithiation can also be found in other reports related to the electrochemical behavior of PDCs [2,4,8]. Table 3 presents a short summary related to the plateau presence/absence during the first lithium insertion, based on the results of the present investigation and on the available literature data.

Furthermore, it should be pointed out that the polysilazane-derived ceramics, HN3 and GM65, recover a significant fraction of the capacity below potentials of 1.5 V. In comparison the discharge curves of the polysilylcarbodiimide-derived SiCN ceramics show that the capacity is recovered over the full potential range. The exact values are gathered in Table 3. The relative recovered capacity below 1.5 V for HN3 and GM65 are in the range of SiOC ceramics as reported by Kaspar et al. [4] and Fukui et al. [2], whereas the values for HN1 and GM35 are in the range of the heat treated SiCN investigated by Feng [8]. In the context of our studies we suggest to discuss this phenomenon in terms of the individual distinct microstructural features of the synthesized SiCN ceramics. ^{29}Si MAS NMR measurements on both SiOC ceramics (PB, SiOC-1100) taken from the literature [2,28] which do not exhibit the plateau show a reasonable amount of mixed bonds which supports the above hypothesis. Solid-state ^{7}Li, ^{13}C, and ^{29}Si-NMR-studies in order to determine if different storing sites and/or a different mobility in polysilazane- and polsilylcarbodiimide-derived ceramics are

Table 3
Absolute and relative capacity recovered during discharge in the 1st and 134th cycle below 1.5 V during discharge.[a]

Sample	Literature data	Plateau at 0.5 V during first charge	1st Discharge below 1.5 V [mA h g^{-1}]	134th Discharge below 1.5 V [mA h g^{-1}]	1st Discharge below 1.5 V [%]	134th Discharge below 1.5 V [%]
HN1		+	507	254	83	68
HN3		–	642	517	91	83
GM35		+	298	202	61	47
GM65		–	639	443	88	75
	Heat treated SiCN [8]	+	410	–	78	–
	PB [2]	–	550	–	92	–
	SiOC_1100 [4]	–	502	–	94	–

[a] For literature values only approximate values for the 1st cycle were taken.

responsible for the variations in the electrochemical performance are currently in progress.

Regarding real applications, the absence of a pronounced two phases region (plateau) as well as the storing ability below a voltage of 0.1 V vs. Li/Li^+ requires the implementation of a voltage-managing device. The materials investigated within this work are therefore especially of interest for large scale applications which are for example used as stationary energy storage devices or in cars.

4. Conclusions

The electrochemical charge/discharge experiments on different carbon-rich polymer-derived SiCN-based ceramics have revealed interesting capacity, cycling stability and capability performance of this class of materials suitable for application in lithium-ion batteries. In particular, the SiCN ceramic derived from the polysilazane HN3 showed an outstanding performance in terms of cycling stability and capacity even at high currents. Furthermore the results demonstrated that a high N/O ratio is not disadvantageous for the electrochemical performance of SiC(O)N ceramics. The use of different classes of precursors does not only lead to different microstructures within the ceramics, but also to differences in the electrochemical behavior. Significant differences in the shape of the first lithiation curves have been measured for the investigated ceramics which is discussed in terms of microstructural features. Accordingly, polysilazane-derived SiCN ceramics exhibit a low delithiation potential as compared to that of polysilylcarbodiimide-derived materials. The amount of branching did not influence the charge and discharge behaviors. The samples HN1, HN3 and GM65 showed an increase in cycling stability with increasing "micropore-activity" which is in agreement with previous studies performed on SiOC ceramics. However, sample GM35 showed the best cycling stability though it did not reveal any lithium storage attributed to closed micropores. Furthermore, no dependence of the capacity on the amount of free carbon was found.

Acknowledgments

We gratefully acknowledge the financial support of the German Research Foundation (DFG) SPP1473, SFB 595/A4 and Materials World Network Program between DFG and National Science Foundation (NSF), as well as the grant funded under the LOEWE-Zentrum AdRIA by the state of Hesse, Germany, and the Fonds der Chemischen Industrie, Frankfurt, Germany.

References

[1] D. Ahn, R. Raj, J. Power Sources 196 (2011) 2179–2186.
[2] H. Fukui, H. Ohsuka, T. Hino, K. Kanamura, ACS Appl. Mater. Interfaces 2 (2010) 998–1008.
[3] M. Graczyk-Zajac, L. Toma, C. Fasel, R. Riedel, Solid State Ionics 225 (2012) 522–526.
[4] J. Kaspar, M. Graczyk-Zajac, R. Riedel, Solid State Ionics 225 (2012) 527–531.
[5] A.M. Wilson, J.N. Reimers, E.W. Fuller, J.R. Dahn, Solid State Ionics 74 (1994) 249–254.
[6] J.R. Dahn, A.M. Wilson, W. Xing, G.A. Zank, U.S.P. US5631106, Dow Corning Corporation, 1997.
[7] D. Su, Y.L. Li, Y. Feng, J. Jin, J. Am. Ceram. Soc. 92 (2009) 2962–2968.
[8] Y. Feng, Electrochim. Acta 55 (2010) 5860–5866.
[9] J. Kaspar, G. Mera, A.P. Nowak, M. Graczyk-Zajac, R. Riedel, Electrochim. Acta 56 (2010) 174–182.
[10] M. Graczyk-Zajac, G. Mera, J. Kaspar, R. Riedel, J. Eur. Ceram. Soc. 30 (2010) 3235–3243.
[11] M. Graczyk-Zajac, C. Fasel, R. Riedel, J. Power Sources 196 (2011) 6412–6418.
[12] L.M. Reinold, M. Graczyk-Zajac, C. Fasel, R. Riedel, ECS Trans. 35 (2011) 37–44.
[13] Y.L. Li, E. Kroke, R. Riedel, C. Fasel, C. Gervais, F. Babonneau, Appl. Organomet. Chem. 15 (2001) 820–832.
[14] Y. Iwamoto, W. Volger, E. Kroke, R. Riedel, T. Saitou, K. Matsunaga, J. Am. Ceram. Soc. 84 (2001) 2170–2178.
[15] P. Colombo, G. Mera, R. Riedel, G.D. Soraru, J. Am. Ceram. Soc. 93 (2010) 1805–1837.
[16] G. Mera, R. Riedel, F. Poli, K. Muller, J. Eur. Ceram. Soc. 29 (2009) 2873–2883.
[17] R.M. Morcos, G. Mera, A. Navrotsky, T. Varga, R. Riedel, F. Poli, K. Muller, J. Am. Ceram. Soc. 91 (2008) 3349–3354.
[18] G. Mera, A. Tamayo, H. Nguyen, S. Sen, R. Riedel, J. Am. Ceram. Soc. 93 (2010) 1169–1175.
[19] Y. Gao, G. Mera, H. Nguyen, K. Morita, H.J. Kleebe, R. Riedel, J. Eur. Ceram. Soc. 32 (2012) 1857–1866.
[20] S. Widgeon, G. Mera, Y. Gao, E. Stoyanov, S. Sen, A. Navrotsky, R. Riedel, Chem. Mater. 24 (2012) 1181–1191.
[21] A.C. Ferrari, J. Robertson, Phys. Rev. B 61 (2000) 14095–14107.
[22] A.C. Ferrari, J.C. Meyer, V. Scardaci, C. Casiraghi, M. Lazzeri, F. Mauri, S. Piscanec, D. Jiang, K.S. Novoselov, S. Roth, A.K. Geim, Phys. Rev. Lett. 97 (2006) 187401–187404.
[23] M.A. Pimenta, G. Dresselhaus, M.S. Dresselhaus, L.G. Cancado, A. Jorio, R. Saito, Phys. Chem. Chem. Phys. 9 (2007) 1276–1291.
[24] A.C. Ferrari, Solid State Commun. 143 (2007) 47–57.
[25] L.G. Cancado, K. Takai, T. Enoki, M. Endo, Y.A. Kim, H. Mizusaki, A. Jorio, L.N. Coelho, R. Magalhaes-Paniago, M.A. Pimenta, Appl. Phys. Lett. 88 (2006) 163106-1–163106-3.
[26] G.A. Zickler, B. Smarsly, N. Gierlinger, H. Peterlik, O. Paris, Carbon 44 (2006) 3239–3246.
[27] R. Saito, A. Jorio, A.G. Souza, G. Dresselhaus, M.S. Dresselhaus, M.A. Pimenta, Phys. Rev. Lett. 88 (2002) 27401–27404.
[28] S.J. Widgeon, S. Sen, G. Mera, E. Ionescu, R. Riedel, A. Navrotsky, Chem. Mater. 22 (2010) 6221–6228.